Journal of Molecular Catalysis A: Chemical 398 (2015) 149–157

Contents lists available at ScienceDirect

Journal of Molecular Catalysis A: Chemical

journal homepage: www.elsevier.com/locate/molcata

Hydroxylation of benzene to phenol over magnetic recyclable nanostructured CuFe mixed-oxide catalyst

Peter R. Makgwane[a,*], Suprakas Sinha Ray[a,b,**]

[a] DST-CSIR National Centre for Nanostructured Materials, Council for Scientific and Industrial Research, Pretoria 0001, South Africa
[b] Department of Applied Chemistry, University of Johannesburg, Doornfontein 2028, South Africa

A R T I C L E I N F O

Article history:
Received 1 April 2014
Received in revised form
13 November 2014
Accepted 22 November 2014
Available online 5 December 2014

Keywords:
Copper
Iron
Nanostructured
Oxidation
Hydroxylation
Benzene
Phenol

A B S T R A C T

A highly active and magnetically recyclable nanostructured copper–iron oxide (CuFe) catalyst has been synthesized for hydroxylation of benzene to phenol under mild reaction conditions. The obtained catalytic results were correlated with the catalyst structure, which was characterized by XRD, SEM, TEM, EDX, H_2-TPR and BET. The catalytic results indicated that the CuFe mixed oxide samples exhibited superior performance compared to its analogous single nano-oxide catalysts. The influence of the reaction condition variables, such as the solvent, reaction temperature, time, and amount of H_2O_2 oxidant, were investigated. Under optimized conditions, CuFe resulted in benzene conversion of 44% at a phenol selectivity of 91% and a corresponding combined hydroquinone/catechol/benzoquinone selectivity of 9%. In addition, the catalytic activity of the nano-oxide CuFe was significantly affected by the different calcination temperatures due to the induced catalyst structure, which was confirmed by the characterization results. This enhanced activity was due to the structural phases and redox modification resulting from the interface between the Cu and Fe metals, which was caused by varying calcination temperatures. The activity of CuFe does not require the formation of the typical favored $CuFe_2O_4$ spinel to achieve a highly active catalyst, which results from the enhanced redox potentials. CuFe is highly recyclable due to its magnetic nature, which results in an excellent ecofriendly catalyst for the direct synthesis of phenol from benzene hydroxylation.

© 2014 Elsevier B.V. All rights reserved.

1. Introduction

From an economic and environmental standpoint, the direct synthesis of phenol from benzene hydroxylation has attracted much research attention in recent years [1–3]. The current commercial production of phenol involves a non-catalyzed chemical reaction based on the Hock process of cumene liquid-phase oxidation, which consists of the preparation of cumene from benzene isopropylation and oxidation of cumene to cumene hydroperoxide (CHP) followed by acid-cleavage decomposition of CHP into phenol and acetone as a side product by H_2SO_4 [4,5]. The disadvantage of this process is that the oxidation is carried out in a series of cascaded bubble-column reactors operated at 5–10 bar and 100–130 °C in the presence of an aqueous basic Na_2CO_3 salt [5], which results in high process costs and a negative impact on the environment due to the generated waste metal salt. In addition, the cumene conversion to CHP is limited to 25–30% to ensure low formation of by-products, such as dimethylphenylcarbinol and acetophenone [4]. However, the use of mineral acids, such as H_2SO_4, in the acid cleavage step typically generates hazardous waste metal salts that are difficult to dispose of. With the continuing demands for green and sustainable chemical conversion protocols, the development of improved catalytic processes utilizing environmentally friendly oxidants (e.g., H_2O_2, TBHP, and O_2) are desirable.

Numerous heterogeneous catalysts based on iron (Fe) oxide have been investigated for their catalytic activity to develop a benzene hydroxylation process that would provide a direct synthetic route to phenol [6–9]. The activity of the Fe catalyst stems from its ability to operate as a Fenton reagent (Fe^{2+}/Fe^{3+}) with H_2O_2 by mediating the catalyzed liquid-phase oxidation reactions to produce highly reactive free-radical oxygen species (i.e., $^{\bullet}OH/HO_2^{\bullet}$) [10,11]. Bianchi et al. [12] developed a biphasic reaction system using $FeSO_4$ for the conversion of benzene in a hydroxylation process that exhibited remarkable phenol selectivity of 97% but at low substrate conversions. This was better when compared to those in

---

* Corresponding author. Fax: +27 12 841 2229.
** Corresponding author at: DST-CSIR National Centre for Nanostructured Materials, Council for Scientific and Industrial Research, Pretoria 0001, South Africa. Tel.: +27 12 841 2388; fax: +27 12 841 2229.
E-mail addresses: pmakgwane@csir.co.za (P.R. Makgwane), rsuprakas@csir.co.za (S.S. Ray).

http://dx.doi.org/10.1016/j.molcata.2014.11.023
1381-1169/© 2014 Elsevier B.V. All rights reserved.

the single phase using other organic solvents. In other studies, Song et al. [13] reported the activity of multi-walled carbon nanotube (MWCNT) supported Fe_3O_4 nanoparticles as a highly active catalyst that was better than Fe supported on conventional supports, such as Al_2O_3 [14], MCM-41 [15], TiO_2 [16], and ZSM-5 zeolites [17], for benzene hydroxylation. In addition, the activity of Fe dispersed on a MgO basic support was also investigated for benzene hydroxylation, and Fe/MgO exhibited nearly the same catalytic performance as that over Fe/Al_2O_3 [14,18]. The most important aspect of these Fe based catalysts is that they all allow the simple green catalytic conversion of benzene to phenol. However, these catalysts primarily afforded low benzene substrate conversions. The low conversions obtained for some of the Fe catalysts may be due to the inactivity of the supports, such as MgO or Al_2O_3. Therefore, the search for new catalysts with improved conversion rates for the benzene hydroxylation to phenol remains an important research challenge. In the benzene hydroxylation reaction, the challenge is to achieve high substrate conversion while maintaining phenol selectivity due to its highly reactive nature that can result in other side products, such as dihydroxybenzene compounds, that may eventually complicate the product separation work-up.

The applications of multicomponent solid catalysts synthesized at the nanosize atomic scale have recently emerged as promising active materials for catalyzing various organic chemical transformations [19,20]. These mixed oxides possess distinct structural properties with better activity than those of their individual counterparts. The resulting enhanced activity has been attributed to interactions that improve the electron charge transfer exchange during chemical reactions [21,22]. In particular, the nano-structural effects are induced by the tailored metal's physico-chemical properties, such as size, morphology, pores, defects, compositions, and interactions [22]. Because the high activity of Fe oxide for liquid-phase oxidations is facilitated by its excellent exchangeable redox cycle with the valence state of Fe^{2+}/Fe^{3+}, the stabilization and mobility enhancement of such species would be important. In addition, one aspect that has been overlooked is the contribution effect from the different Fe oxides phases (i.e., Fe_2O_3, Fe_3O_4, and FeO) on its catalytic performance in liquid-phase oxidations [23,24]. Although Fe is active for oxidation reactions, its use in liquid-phase oxidations has been primarily limited to soluble homogeneous catalysts immobilized on various ligands [25–28]. However, the problem with homogeneous designed catalyst systems is their poor recyclability and rapid deactivation, which hinders their ultimate application in industrial oxidation processes. However, heterogeneous solid Fe catalysts exhibit enormous benefits related to environmental sustainability and process economics due to enhanced recyclability. Therefore, the hetero-mixing of Fe oxide with another metal oxide that possesses an excellent redox cycle would result in a highly active catalyst for liquid-phase oxidation reactions. In fact, Fe would provide the catalytic activity as well as the recyclability due to its magnetic recoverable properties in the liquid phase. Catalysis using copper (Cu) oxides is well established in the literature for liquid-phase oxidations of hydrocarbons and alcohols [29–33]. In addition, Cu also possesses an interesting redox cycle (Cu^{2+}/Cu^{+}) that is amenable to facilitating free-radical oxidation reactions. Therefore, the combinations of Fe and Cu metals provide an opportunity to further explore their hetero-mixed catalytic properties for the oxyfunctionalization of typical benzylic hydrocarbons C—H in liquid-phase oxidations.

The challenge in the preparation of such nanostructured hetero-mixed metal oxides is to ensure that the synthetic method produces uniform nanoparticles with the desired interaction and exposed active sites. The polylol synthetic method using a co-precipitation approach for structuring more than two combined metals in the presence of a polymer surfactant as a structure templating agent has been extensively studied [34]. Yang et al. [35] reported the versatile synthesis of the CuFe composite with a rod-like nanoparticle morphology using a polyvinyl pyrrolidine (PVP) surfactant in ethylene glycol (EG), which served as both the solvent and reductant. Kenfack and Langbein [36] reported that the formation of the spinel structure properties of $CuFe_2O_4$ is temperature dependent and the CuFe catalytic performance is sensitive to the structural phase. Yan and Chen [37] demonstrated the enhanced catalytic performance of nanostructured CuFe with different compositions for the hydrogenation of biorenewable furfural and levulinic acid [38]. The activity of the CuFe composite was also evaluated for the liquid-phase oxidation of toluene to benzaldehyde as the major reaction product by Wang et al. [39]. The nanostructure CuFe composite exhibited efficient catalytic activity and high magnetic recyclability in the Friedel–Craft acylation for the organic chemical transformation in the synthesis of biologically active moieties [40] High catalytic activity and excellent catalyst stability was reported for Ullmann C—O coupling reactions catalyzed by magnetic copper ferrite (CuFe) nanoparticles with high yields for the targeted chemical products [41].

Despite the successful catalytic activity exhibited by CuFe based catalysts in different liquid-phase reactions and environmental cleaning, its application for benzene hydroxylation has not been reported. Not only can nanostructured CuFe composite materials provide a highly active catalyst for the activation of the C—H bond in benzene for selective oxygen introduction but the catalyst system can be sustainable due to its less expensive metals and their natural abundance. Herein, we report the synthesis of a nano-oxide copper–iron (CuFe) composite material with interesting structure-dependent catalytic activity performance, which was induced by the calcination temperatures, in the hydroxylation reaction of benzene for the direct synthesis of phenol. The synthesized CuFe catalyst was catalytically active and magnetically recoverable in this reaction. The structural features of the prepared catalysts were investigated using X-ray diffraction (XRD), hydrogen-temperature programmed reduction (H_2-TPR), high-resolution transition electron microscopy (HRTEM) coupled to energy dispersive X-ray (EDX), field emission scanning electron microscopy (FESEM), and N_2 physisorption.

2. Experimental section

2.1. Catalyst preparation procedure

The synthesis of the nanostructured CuO, Fe_3O_4, and $CuFe_2O_4$ catalyst materials were prepared by the polylol method using ethylene glycol (EG) as the solvent and a poly (vinyl pyrrolidine) (PVP) surfactant. Typically, $Cu(NO_3)_2{\cdot}6H_2O$ (5 mol, Cu metal) and 5 mol of a mixture of $Fe(III)Cl_3{\cdot}6H_2O$ and $Fe(II)SO_4$ in in a 1:1 molar ratio were dissolved in ethylene glycol (70 mL). In addition, 1.0 g of PVP was added as a structure directing templating agent. The mixture was stirred vigorously for 30 min, and then, the pH of the reaction was adjusted to 12 using ammonium hydroxide (NH_4OH, Aldrich). The materials were aged for 24 h under reflux. Similarly, the respective individual oxides of Cu and Fe were prepared following the same procedure. The prepared catalyst was vacuum filtered and washed several times with ethanol prior to drying in air for 12 h at 100 °C. The prepared CuFe catalyst was calcined under oxidation conditions at different temperatures with a heating rate of 10 °C/min, and the calcination temperature was maintained for 4 h. The prepared catalysts are denoted CuFe-300, CuFe-400, CuFe-500, and CuFe-600 depending on the calcination temperature used. Based on the better catalytic results obtained for CuFe-400, we also calcined the individual catalysts at 400 °C (Cu-400 and Fe-400) for comparison of their activity with the CuFe-400 composite.

2.2. Catalyst characterization procedures

The total specific surface area as well as the micropores volume and areas of the catalysts were measured by nitrogen (N_2) physisorption at 77 K using a Micromeritics TRISTAR 3000 surface area analyzer (USA). Prior to analysis, the samples were degassed at 120 °C for 12 h under a continuous flow of N_2 gas to remove adsorbed contaminants. The XRD experiments were recorded on a PAnalytical XPERT-PRO diffractometer using Ni filtered CuKα radiation ($\lambda = 1.5406$ Å) at 40 kV/50 mA. The diffraction measurements were collected at room temperature in a Bragg–Brentano geometry with a scan range of $2\theta = 10–90°$ using continuous scanning at 0.02°/s. TEM measurements were performed by a JEOL JEM 2100 operated at an accelerating voltage of 200 kV. The powder samples were sonicated for 5 min in ethanol and dispersed on a copper grid for TEM analysis. The elemental analysis of the different metals was simultaneously determined using EDX coupled to the TEM. H_2-TPR studies were performed on a Micromeritics Autochem AC2920 apparatus (USA). The reduction of the catalyst samples was carried out under a gaseous mixture of 10% H_2/Ar at a heating rate of 10 °C/min from 50 to 800 °C and a total gas flow rate of 50 ml/min. Prior to starting the H_2-TPR measurements, the samples were precleaned for approximately 1 h at 70 °C using an argon gas flow. The H_2 consumption was monitored by a calibrated thermal conductivity detector (TCD). The microstructure surface morphologies of the catalysts were characterized by FESEM (JEOL). Prior to analysis, the samples were sputter coated with gold to minimize their possible charging.

2.3. Catalytic testing

The catalytic reactions were performed in a 50 ml two-necked round-bottom flask equipped with a reflux condenser, magnetic stirrer, and thermometer. The catalyst (50 mg) and benzene (10 mmol) in solvent (5 ml) were combined and maintained under stirring at 70 °C for 5 min prior to slowly adding the aqueous 50% H_2O_2 (30 mmol) oxidant. The reaction was continued for 4 h at a constant temperature, which was controlled using an oil bath. After 3 h, the reaction was terminated and cooled prior to analyzing the products on an Agilent Gas Chromatograph (GC) A6890 equipped with a split inlet (250 °C, split ratio of 100) using SPB 20 capillary column (30 m × 25 μm × 0.25 mm ID) at a constant flow of carrier gas coupled to a flame ionization detector (FID). The elution temperature of the oven components was ramped from 80 °C (3 min, hold-up time) to 220 °C at a heating rate of 10 °C/min. Nitrobenzene was used as the internal standard for quantification of the components, which were identified using authentic standards purchased from Aldrich. For the CuFe catalyst recyclability studies, after each reaction cycle, the catalyst was separated using an external magnet, and the new reaction liquids were added to start the next recyclability reaction cycle.

3. Results and discussion

3.1. Catalyst characterization

3.1.1. XRD crystalline structure characterization

To understand the structural characteristics of the nanosynthesized CuFe composite, wide-angle powder XRD was used to identify the phases and crystallinity of the catalyst samples. The obtained XRD patterns of the CuFe catalysts calcined at different temperatures including the individual nano-oxides of Cu and Fe are shown in Fig. 1. For copper oxide nanostructure, the XRD diffraction peaks $2\theta = 32.4°$, 35.5°, 38.7°, 48.7°, 53.2°, 57.9°, 61.3°, 66.1°, 68.0°, 71.9°, and 74.8° corresponding to the crystal structure of the CuO phase were determined to matched the (1 1 0), (0 0 2), (1 1 1), (2 0 2), (0 2 0), (2 0 2), (1 1 3), (0 2 2), (2 0 0), (3 1 1), and (2 2 2) plane reflections. Similarly, the formation of typical iron magnetite Fe_2O_4 diffraction patterns at $2\theta = 30.3°$, 35.6°, 43.2°, 53.4°, 57.2°, and 62.7° was confirmed by XRD analysis to correspond to the (2 2 0), (3 1 1), (4 0 0), (4 2 2), (5 1 1), and (4 4 0) reflection planes of the face-centered cubic phase of Fe_3O_4 [42]. The CuFe catalyst samples calcined at both 300 and 400 °C exhibited similar XRD structural patterns. For CuFe-300 and CuFe-400, all of the XRD peaks were indexed to the respective CuO and Fe_3O_4 phases. However, the peak intensities corresponding to CuO in the CuFe-300 and CuFe-400 composite materials compared to the XRD of pure CuO were low while those belonging to Fe_3O_4 were high and clearly visible. Notably, as the CuFe calcination temperature increased to 500 and 600 °C, the formation of additional XRD peaks at $2\theta = 25.3°$, 34.7°, 49.5° 58.8°, 63.7°, and 71.6° started to appear. These peaks indicated the formation of the $CuFe_2O_4$ spinel structure phase. In addition, the presence of XRD peaks at $2\theta = 34.7°$ and 35.9° represent the formation of the $CuFe_2O_4$ spinel structure with a tetragonal phase [36]. The intensity of the peak at $2\theta = 34.7°$ increased as the calcination temperature increased from 500 to 600 °C. There was an additional peak that appeared at 41.9° in the XRD patterns for the CuFe-500 and CuFe-600 catalysts that was not observed in the CuFe-300 and CuFe-400 catalysts. This peak was attributed to the formation of the α-Fe_2O_3 phase of the iron compounds associated with the $CuFe_2O_4$ spinel structure transformation. Another noticeable effect of temperature on the structure of the CuFe composite material was the gradual increase of the overlapping peaks corresponding to both Cu and Fe at $2\theta = 35.9°$ as the calcination temperature increased. This result indicated particle sintering or ordering of the CuFe structure accompanied by the possible crystallite size growth. Correspondingly, based on the values of the full-width at half-maximum (FWHM) for the strong XRD peaks, the crystallite size of the particles were estimated using the Scherrer equation. As shown in Table 1 with the physical characterization data of the nanostructured catalysts, the grain size of the nanoparticles increased as the calcination temperature increased beginning with the as-prepared CuFe composite material dried at 100 °C.

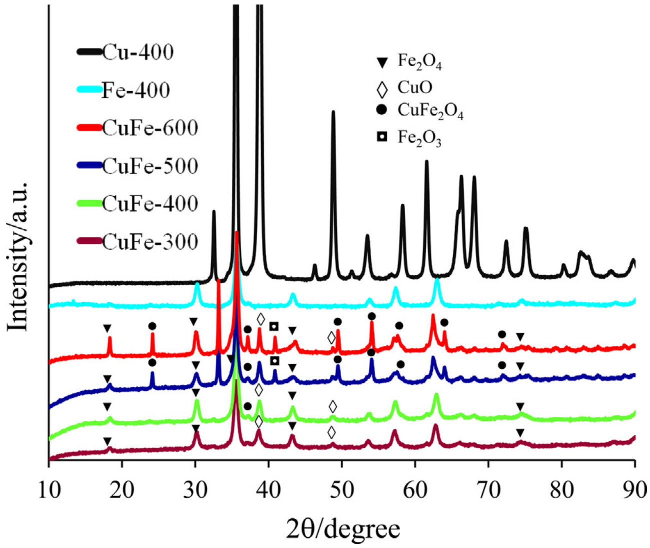

Fig. 1. XRD patterns of the copper–iron based nanostructured catalysts.

3.1.2. N_2 physisorption characterization

The physical characterization data of the catalysts are reported in Table 1. The CuO and Fe_3O_4 catalysts calcined at 400 °C possessed a surface area of 58.0 and 23.4 m^2/g, respectively, and the CuFe

Table 1
Physical characterization data of the nanostructured Cu and Fe based catalysts.

Entry	Catalyst	BET surface area (m^2/g)	Micropores volume (cm^3/g)	Micropores area (m^2/g)	Particles size (nm)[a]
1	Cu-400	23.4	0.36	17.6	14.4
2	Fe-400	58.0	0.41	21.3	13.6
3	CuFe-300	44.4	0.35	14.6	15.9
4	CuFe-400	33.7	0.33	10.5	17.4
5	CuFe-500	18.1	0.20	8.3	19.3
6	CuFe-600	5.1	0.07	2.3	23.4

[a] Estimated from XRD results using the Scherrer equation.

mixed oxide, which was also calcined at 400 °C, possessed a surface area of 33.7 m^2/g, which is in between the two values for the CuO and Fe_3O_4 catalysts. The calcination of CuFe at different temperatures over a range of 300–600 °C induced significant changes in the BET surface area of the materials, which ranged from 44.4 m^2/g (300 °C) to 5.1 m^2/g (600 °C). This relative drop in the CuFe surface area with temperature indicated possible grain size growth leading to the structural morphology of the nanoparticles becoming stacked together decreasing their surface area, as discussed later with the FESEM results (Fig. 2). The catalyst micropore volumes and areas corresponded to the obtained changes in the samples surface areas, which indicated that the structural modification of the physicochemical properties of the catalysts resulted from the interaction of CuO and Fe_3O_4 as well as the effect of the calcination temperature. The low micropore volume of the CuFe-600 sample compared to other CuFe catalysts may be related to its different porosity nature, as shown by the FESEM images (Fig. 3a–g)

3.1.3. *TEM and SEM morphology characterization*

To investigate the calcination temperature-induced morphological evolution of the CuFe mixed oxides catalyst, FESEM and TEM were used to analyze the structural morphological development of the catalyst during a series of thermal treatments (i.e., 300–600 °C). The recorded low and high magnification FESEM images of the catalyst morphologies are shown in Fig. 2a–i. For the as-prepared CuFe and calcined CuFe at 300 °C, the formation of disconnected particles were observed compared to the slightly agglomerated morphology for the CuFe catalysts calcined at 500 °C and 600 °C. Both the high magnification images of the as-prepared CuFe and that calcined at 300 °C indicated the formation of uniform nanosized particles with an average size of 30–50 nm (Fig. 2b and d). With a further increase in the calcination temperature to 600 °C, a completely different morphology was observed compared to the other calcination temperatures (Fig. 2e–g). The disconnected particle morphology obtained for CuFe calcined at 300–500 °C became stacked together

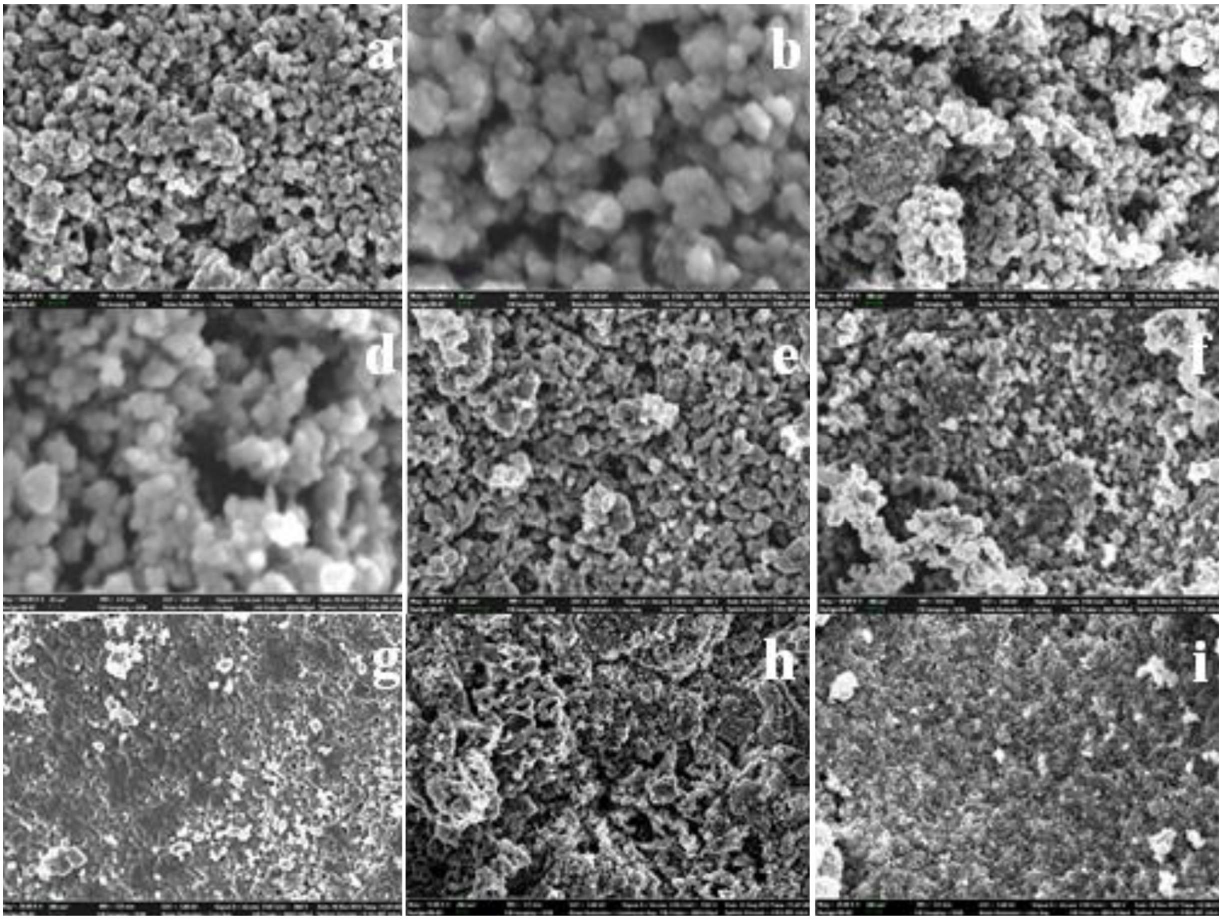

Fig. 2. SEM images for (a) the as-prepared CuFe, (b) high magnification of the as-prepared CuFe, (c) CuFe-300 (d) high magnification of CuFe-300, (e) CuFe-400, (f) CuFe-500, (g) CuFe-600, (h) Cu-400 and (i) Fe-400. High magnification: ×140 000 at 30 nm scale bar for (b) and (d).

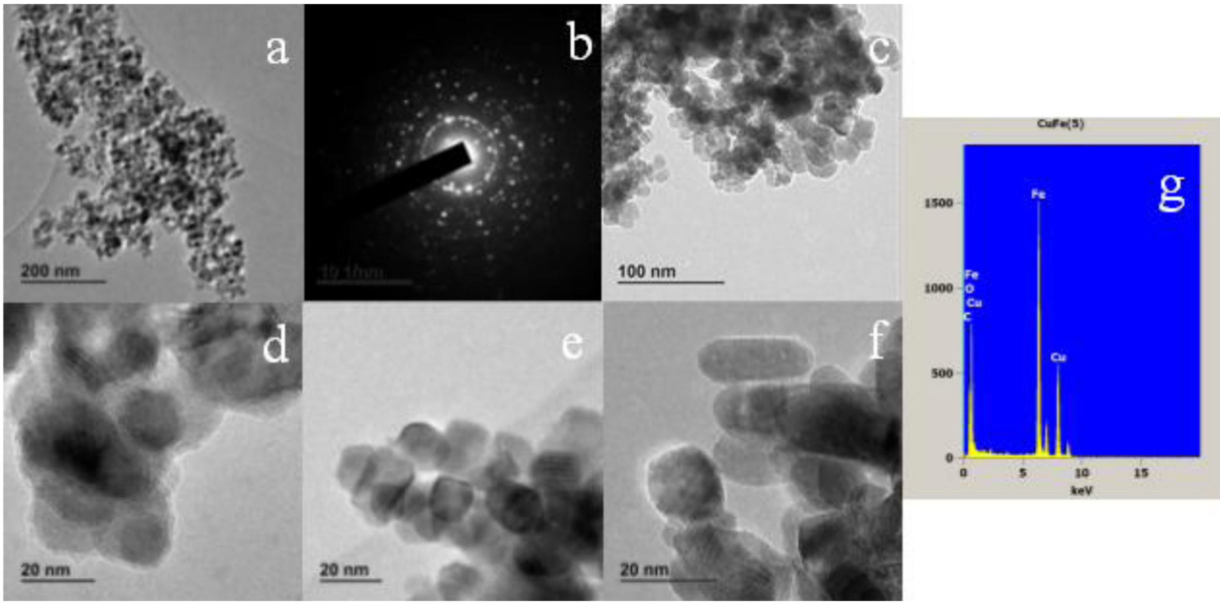

Fig. 3. TEM image (a) and SAED (b) of CuFe-400, (c) enlarged CuFe-400 from (a), high resolution TEM images of (d) CuFe-400, (e) Fe-400, (f) Cu-400 and (g) EDX for CuFe in Fig. 3c.

forming a continuous rough surface at 600 °C. This drastic morphological change in CuFe as the temperature increased to 600 °C was confirmed by the XRD phase changes where the separate CuO and Fe_3O_4 phases at 300 °C and 400 °C were converted into the spinel $CuFe_2O_4$ structure phase for CuFe calcined at 500 °C and 600 °C. For individual CuO and Fe_3O_4 nano-oxides calcined at 400 °C, both nano-oxides formed distinctive particle shape morphologies that were porous compared to the CuFe catalysts.

The representative morphology observed in the TEM images of the CuO and Fe_3O_4 nano-oxides as well as selected CuFe composite samples calcined at 400 °C are shown in Fig. 3a–g. The TEM and HRTEM images of CuFe-400 indicated the formation of a uniform nanosized particle shape (Fig. 3a and b). The selected area electron diffraction (SAED) pattern of the synthesized nanostructured CuFe-400 composite catalyst is shown in Fig. 4c. The well-defined concentric rings displayed in the SAED patterns support the nanocrystalline nature of the synthesized material, which correlates with the obtained XRD results (Fig. 1). For the CuFe composite, the formation of particles with a morphology that was similar to the individual catalyst oxide samples was observed (Fig. 3d). According to the HRTEM images, the pure Fe_3O_4 catalysts were comprised of irregular nanospherical shaped particles with an estimated nanosize of approximately 10–30 nm. In addition, CuO was composed of a spherical and octahedral shaped morphology (Fig. 3e and 3f). The EDX spectra of the CuFe-400 catalyst shown in Fig. 3g confirmed the presence of Cu (44%) and Fe (56%) metal in the composite catalyst sample with.

3.1.4. H_2-TPR chemisorption characterization

The reactivity of the mixed and single oxide CuFe catalyst surfaces was examined by studying oxygen removal under hydrogen (H_2) reduction conditions. Fig. 4 shows the redox properties of the catalysts characterized by H_2-TPR. The H_2-TPR curves of CuO indicated a one-step reduction of $Cu^{+2} \rightarrow Cu^0$ centered at 244 °C. The Fe nano-oxide exhibited two reduction peaks in the temperature range of 200–300 and 350–800 °C, which indicated that the reduction of Fe_3O_4 involved a multiple-step reduction to the metallic Fe phase. The initial peak was sharp and centered at 315 °C, and the high temperature reduction peak was broad and stretched over a wide temperature range. The TPR profiles of the CuFe catalysts calcined at different temperatures exhibited distinct reduction peak patterns that were categorized by three different reduction temperatures at 50–250 °C, 250–450 °C, and 450–800 °C. First, at a reduction temperature below 300 °C, CuFe-400 exhibited high reactivity to the surface oxygen removal initiated by the reduction of CuO to Cu compared to the other CuFe mixed oxide catalysts calcined at different temperatures. Therefore, a shift in the reduction temperature of Cu to a low region based on the calcination temperature effect decreased in the following order: CuFe-400 (T_{max} = 176.9 °C) < CuFe-300 (T_{max} = 182.4 °C) < CuFe500 (T_{max} = 260.5 °C) < CuFe-600 (T_{max} = 225.3 °C). It is important to note that the difference in the peak reduction intensities corresponding to CuO at 300 °C was poor for CuFe-600 compared to the other nano-oxides CuFe catalysts. In addition, this low reduction peak also exhibited a slight shift in reduction temperature accompanied by a multiple-stage reduction compared to the single reduction peak of CuO observed in the other CuFe catalysts that were calcined at 300, 400 and 500 °C. By comparing the H_2-TPR data for a reduction temperature of less than 300 °C to the FESEM morphologies of the CuFe catalysts, it is reasonable to suggest that the particle agglomeration observed in CuFe-600 could have resulted in the coverage of the copper species by iron oxide, which could make their reduc-

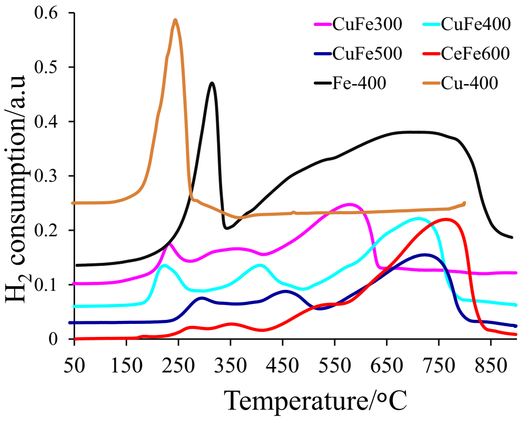

Fig. 4. H_2-TPR profiles of the different copper–iron based nanostructured catalysts.

Table 2
Catalytic performance of the Cu and Fe based catalysts for benzene hydroxylation.

Entry	Catalyst	Benzene conversion (%)	Selectivity (%)					H_2O_2 efficiency (%)
			Phenol	HQ[a]	CAT[b]	BQ[c]	Others	
1	Blank	–	–	–	–	–	–	–
2	Cu-400	4.3	75.4	7.8	6.5	6.0	4.3	87.6
3	Fe-400	12.6	77.2	5.6	4.1	10.1	3.0	89.6
4	CuFe-300	29.2	89.3	4.5	3.2	3.0	–	91.5
5	CuFe-400	38.4	92.4	3.6	2.6	1.4	–	93.0
6	CuFe-500	23.0	81.4	12.7	3.1	2.8	–	88.9
7	CuFe-600	20.0	72.4	15.3	2.3	5.4	4.6	86.7
8[d]	CuFe-400	26.4	94.3	2.5	2.0	1.2	–	92.3

Reaction conditions: Benzene (10 mmol); catalyst (50 mg), 50% H_2O_2 (30 mmol), acetonitrile solvent (5 ml), reaction temperature (70 °C) and reaction time (4 h).

[a] HQ – hydroquinone.

[b] CAT – catechol.

[c] BQ – benzoquinone.

[d] The control reaction was carried out with 30% H_2O_2 oxidant.

tion slightly difficult or incomplete. This result was also confirmed by the multiple-stage reduction of the CuFe-600 catalyst sample compared to the other CuFe catalysts calcined at different temperatures. It is possible that this result indicates the presence of Cu particles with different sizes that will require different reduction temperatures. An additional impact of the calcination temperature on the reduction of the different CuFe catalysts was clearly visible in the reduction temperature shift of the peaks at 500–850 °C for all of the CuFe mixed oxide catalysts. The CuFe catalysts calcined at 300 and 400 °C exhibited slightly low reduction temperatures for the reduction of the FeO phase to metallic Fe compared to CuFe-500 and CuFe-600. The observed variations in the CuFe reduction patterns resulting from different calcination temperatures can have a significant influence on the catalytic performance of the catalyst. The shift in the reduction temperatures according to the different calcination temperature of mixed CuFe oxide catalyst was previously observed by Xiao et al. [43].

3.2. Catalytic activity evaluation

3.2.1. Catalysts activity screening

The direct hydroxylation of benzene into phenol and the corresponding dihydroxybenzene derivatives constitute one of the important chemical reaction processes in liquid-phase oxidations. Therefore, we carried out the benzene oxidation reaction using aqueous H_2O_2 as the terminal oxidant to evaluate the catalytic activity of the nanostructured CuFe based catalysts. Table 2 lists the obtained catalytic results for the different CuFe catalysts. The non-catalyzed reaction resulted in no benzene substrate conversion after 4 h irrespective of the addition of the highly reactive H_2O_2 oxidant. However, for catalyzed reactions using the CuFe catalysts, benzene substrate conversions of up to 38% were achieved under similar reaction conditions. Among the evaluated catalysts, CuFe calcined at 400 °C exhibited the highest benzene conversion. This conversion for the CuFe-400 catalyst was better than that obtained with the individual CuO and Fe_2O_4 catalysts under the same reaction conditions. Overall, in terms of the benzene conversion efficiency, *t* an increasing order of performance was observed as follows: CuFe-400 > CuFe-300 > CuFe-500 > CuFe-600 > Fe-400 > Cu-400 (Table 2). This trend indicated the significant catalytic effect exerted by the CuFe mixed oxide catalyst depends on the calcination temperatures due to the various induced structural characteristics. For example, CuFe-400, which exhibited the best performance, was composed of the Fe_3O_4 phase, and CuFe-600 consisted of a mixture of Fe_3O_4 and Fe_2O_3 iron phases in addition to the spinel $CuFe_2O_4$ structure phase (Fig. 1). Representative catalysed benzene hydroxylation reaction with typical industrial used aqueous H_2O_2 with content of 30% was carried out (Table 2, entry 8). It can be seen that the comparison of CuFe-400 with 50% H_2O_2 exhibited high catalytic performance when compared to 30% H_2O_2. This could be ascribed to the possible effect of saturated H_2O_2 with little water effect of 50% compared to 70% in the H_2O_2 that might create competitive adsorption of benzene and water at the catalyst active sites, thus slightly lowering the catalyst activity. This issue is also discussed later on the effect of solvent, where water was used as the solvent (Section 3.2.2). The selectivity with respect to H_2O_2 efficiency to product formation was found to be slightly better for the CuFe-300 and CuFe-400 catalysts. As shown in Table 2, the catalytic conversion of the CuFe catalysts was initially high for calcination temperatures of up to 400 °C and the decreased significantly at 500 and 600 °C. These observations may be related to the mixed oxide catalyst structural characteristics, such as redox properties (H_2-TPR Fig. 4), and the respective particles morphological and phase transformation exhibited by the CuFe composite catalysts as the calcination temperature increased (XRD, Fig. 1 and FESEM, Fig. 2). According to the SEM images (Fig. 2), the CuFe catalysts calcined at 500 and 600 °C exhibited morphology with highly agglomerated particles with a continuous smooth surface. This transformation in catalyst's morphology was accompanied by significant changes in porosity and particles size. As results, it is possible that this type of morphology for CuFe-500 and CuFe-600 could hinder the active catalyst sites, which could make it difficult for the reaction species to access them compared to the high catalytic performance exhibited by the CuFe-300 and CuFe-400 catalysts, which have loose particles that are more porous. As previously mentioned, the best performing catalyst was composed of Fe_3O_4 and CuO phases rather than the $CuFe_2O_4$ spinel. Therefore, it is reasonable to suggest that in the current study, the spinel structural formation of the $CuFe_2O_4$ phase is not the only requirement for achieving an active catalyst capable of oxidizing the typical inert benzene C—H bond to oxygenates. It is also important to note that the catalytic activity of CuFe calcined at various temperatures exhibited different H_2-TPR surface oxygen reactivity, which indicated the significant structural modification effect on the composite catalyst redox cycles of the two metals. This result is consistent with the low reduction temperatures (i.e., H_2-TPR) of the CuFe-300 and CuFe-400 catalysts samples exhibited high catalytic performance compared to CuFe-500 and CuFe-600, which exhibited a slight high H_2-TPR temperature shift. Therefore, the correlation of the catalytic and characterization results clearly demonstrated the significant influence of the calcination temperature on the CuFe mixed-oxide for achieving a highly active catalyst with enhanced exposed catalytic sites. In addition to the better benzene conversions achieved with the CuFe-300 and CuFe-400 catalysts, these catalysts afforded good phenol selectivity compared to the CuFe-500 and CuFe-600 catalysts (Table 2). To investigate if the redox cycle structure of

Table 3
Effect of different solvents on the catalytic performance of the Cu and Fe based catalysts.

Entry	Solvent	Benzene conversion (%)	Selectivity (%)				
			Phenol	BQ[a]	HQ[b]	CAT[c]	Others
1	Acetonitrile	38.4	91.0	3.1	2.5	2.4	–
2	Water	7.4	97.3	0.3	0.4	1.0	–
3	Methanol	45.3	92.8	4.0	1.2	2.0	–
4	Acetic acid	12.4	90.1	5.8	2.6	1.5	–
5	Hexane	–	–	–	–	–	–
6	Ethanol	34.3	93.3	3.1	2.2	1.4	–
7	Propanol	31.7	95.2	2.8	1.5	0.5	–

Reaction conditions: Benzene (10 mmol); catalyst (50 mg), 50% H_2O_2 (30 mmol) acetonitrile solvent (5 ml), temperature (70 °C) and time (3 h).

[a] HQ – hydroquinone.

[b] BQ – benzoquinone.

[c] CAT – catechol.

oxidized CuFe-400 (i.e., Fe$^{+3/+2}$ and Cu$^{+2/+1}$) was the requirement for the high catalytic performance of the catalyst, we tested the activity of reduced CuFe-400 under H_2 together with Fe-400. The details of the reduction conditions and characterisation results are summarized in the supporting information (Fig. S1a and b). The reduced CuFe-400 exhibited low catalytic activity of 5% benzene conversion with 100% phenol selectivity. For reduced Fe-400, no benzene conversion was observed. It is noteworthy to mention that under the 4 h reaction time the oxidized CuFe-400 afforded higher conversion compared to reduced CuFe-400 of less than 1%. The 5% conversion was only achieved after prolonged reaction time of up to 12 h. Furthermore, to exclude any possible self-catalytic effect of benzene/H_2O_2, the blank reaction carried out with both substrates showed no conversion after 12 h. The XRD correlation of fresh and used CuFe-400 (reduced) exhibited significant structural changes of the used catalyst (Fig. S1a and b). We assume that these structural changes after prolonging the reaction time to up to 12 h was accompanied by the formation of the active phase of CuFe-400 from its reduced form that facilitated the operation of efficient redox Fe^{+2}/Fe^{+3} (Fenton-like) for the active catalyst. However, this observation requires further studies to probe the actual influence of the different phases and oxidation state of mixed CuFe oxide catalyst activity.

The effect of the classical Fenton-like catalytic chemistry in the oxidation reactions involving H_2O_2 produces hydroxyl species by the ferrous ion (Fe^{2+}) according to the proposed redox cycle mechanism described below [11].

$$Fe^{2+} + H_2O_2 \rightarrow Fe^{3+} + HO^{\bullet} + OH^{-} \tag{1}$$

$$Fe^{3+} + H_2O_2 \rightarrow Fe^{2+} + HOO^{\bullet} + H^{+} \tag{2}$$

$$Fe^{2+} + HO^{\bullet} \rightarrow Fe^{3+} + OH^{-} \tag{3}$$

In the initial step, H_2O_2 is decomposed by iron to form highly reactive hydroxyl species, which oscillates between Fe^{+2}/Fe^{+3} during the reaction according to Eqs. (1) and (2). These hydroxyl species are capable of attacking the benzene ring C—H bond to form benzylic free radicals that subsequently trap the oxygen species from the available hydroxyl source. Similarly, copper is capable of operating in the same manner as iron in the H_2O_2 catalyzed liquid-phase oxidations according to the equations described below and as indicated by the catalytic results in Table 2.

$$Cu^{+} + H_2O_2 \rightarrow Cu^{2+} + HO^{\bullet} + OH^{-} \tag{1}$$

$$Cu^{2+} + H_2O_2 \rightarrow Cu^{+} + HOO^{\bullet} + H^{+} \tag{2}$$

$$Cu^{+} + HO^{\bullet} \rightarrow Cu^{2+} + OH^{-} \tag{3}$$

It has been proposed that the presence of copper in such a CuFe composite for Fenton-like operation facilitates an enhanced and efficient redox exchange cycle between the Fe^{+2}/Fe^{+3} oxidation states for oxidation reactions. In addition, the copper may also play an active role in the catalyst by accelerating the initiation of the reaction, as observed for the catalytic activity of pure CuO in Table 2. The selectivity of the formed HO/HO_2 hydroxyl species from the Fenton chemistry decomposition has been questioned in the literature, especially the HO_2 species, which is believed to be unselective. Therefore, the potential quantification of such hydroxyl species in the H_2O_2 catalyzed oxidation reactions would allow for the development of Fenton-like oxidation catalysis that would allow for optimization of the selectivity and tuning of the catalyst redox cycles.

3.2.2. Effect of reaction variables on CuFe-400 catalytic performance

After the initial high catalytic activity displayed by the CuFe catalyst calcined at 400 °C during the catalyst screening, we further investigated the influence of the different reaction variables (i.e., solvent, temperature, time and re-usability) on the catalyst performance in the benzene hydroxylation reaction.

Table 3 summarizes the results for the effect of the type of solvent on the catalytic performance for the CuFe-400 catalyst sample. The effect of the solvent in the liquid-phase reactions is important for facilitating the solubility of the reacting species, which enhances the mass transport of their interaction. Therefore, different solvents (i.e., water, methanol, acetonitrile, ethanol, propanol, acetic acid and hexane) were investigated to determine their effect on the catalytic performance of the CuFe-400 catalyst for the hydroxylation of benzene. The nature of the solvent plays a major role in chemical reactions to enhance on reactants solubility, thus improving the mass transfer of reactants contact. It can also increase on conversion and tailor products selectivity significantly. The conversion of benzene as well as the selectivity to phenol varied significantly with the different solvents. Water as protic and immiscible solvent to benzene yielded poor conversion but excellent selectivity for phenol compared to acetonitrile, which exhibited high conversion with a slightly lower phenol selectivity. We believe that water was strongly adsorbed on the catalyst surface active sites, which competed with benzene and H_2O_2, thus lowering the substrate conversion. On the other hand, methanol performed exceptionally well among the evaluated solvents. When the type of alcohol was varied from methanol to propanol, the alcohol with more carbon atoms performed relatively poorly for substrate conversion compared to the C1 alcohol but the selectivity for phenol improved. The high performance of methanol was ascribed to its high polar protic nature and high dielectric constant compared to other alcohols. Under acetic acid conditions, the reaction also exhibited poor substrate conversion, which is most likely due to acceleration of the self-decomposition rate of hydrogen peroxide assisted by the acidic medium catalysis that can lead to a decrease in activity. Water exhibited the lowest catalytic activity but a good phenol selectivity of approximately 97.3%. This result may be due to the reaction

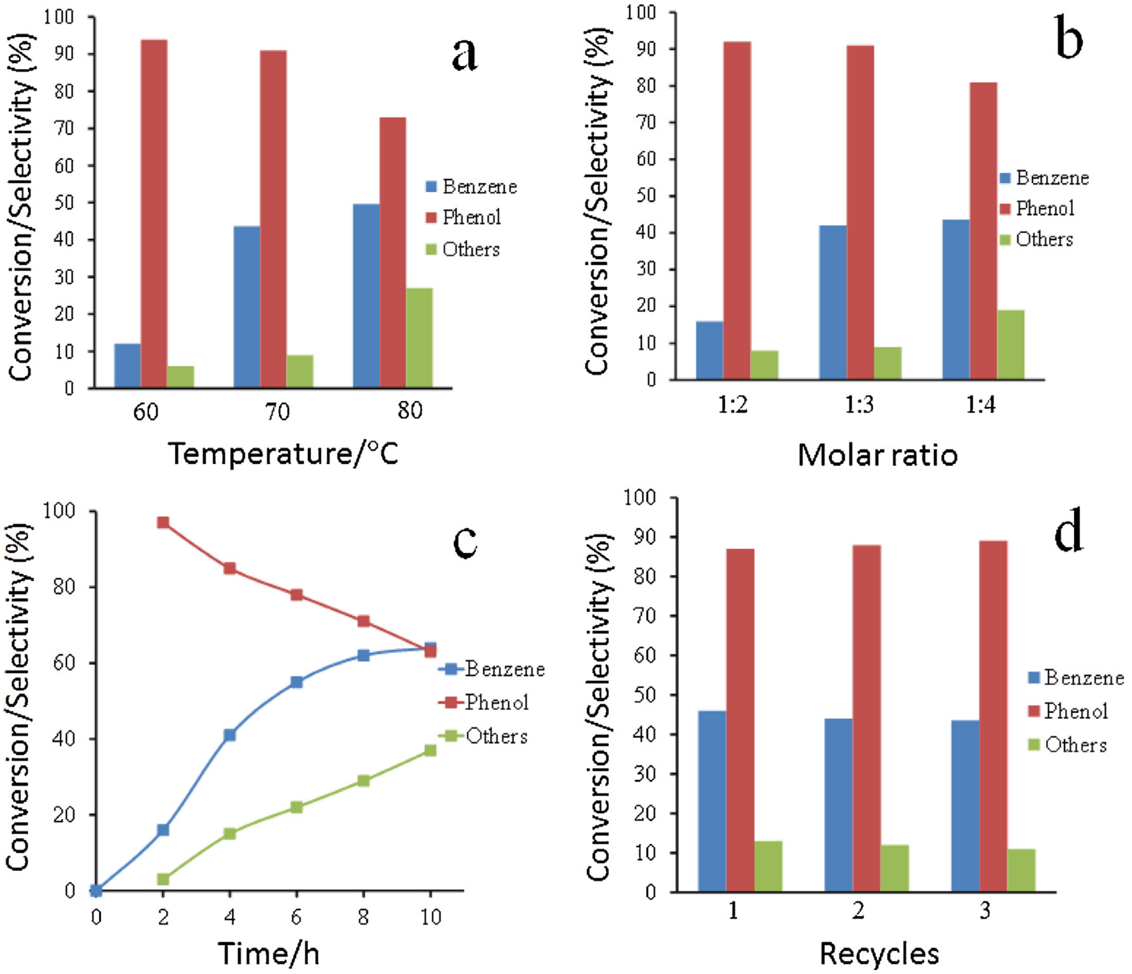

Fig. 5. Catalytic performance of the CuFe-400 catalyst under different reaction conditions. (a) Effect of temperature, (b) effect benzene to H_2O_2 molar ratio, (c) effect of reaction time, and (d) catalytic recyclability test performance. Other reaction conditions: Benzene (10 mmol); catalyst (50 mg), solvent (5 ml).

occurring in a biphasic reaction medium where the products are separated from the active catalyst by the organic and aqueous phase medium. Therefore, catalytic decomposition of the formed phenol is less severe. Bianchi et al. [12] demonstrated that this biphasic strategy is beneficial for improving the selectivity and yield of phenol in the benzene hydroxylation process.

Next, we varied the reaction temperature (i.e., 60–80 °C) while keeping all of the other reaction variables constant. As shown in Fig. 5a, the increase in reaction temperature was beneficial for increasing the oxidation reaction rates as well as the benzene substrate conversion. However, the negative impact of increasing reaction temperature was noticeable on the selectivity to phenol at 80 °C, which decreased to approximately 73%. The over oxidation products, which substantially increased, were identified as hydroquinone, benzoquinone and catechol. Therefore, a temperature of 70 °C was regarded as the optimum required for reasonable oxidation rates with appreciable preservation of a phenol selectivity of approximately 90%. Fig. 5b shows the effect of varying the concentration of the H_2O_2 oxidant in the range of 2–4 molar ratios to benzene on the conversion and product selectivity in the hydroxylation of benzene. According to the obtained results, a high H_2O_2 concentration resulted in a decrease in the phenol selectivity, which promoted the formation of the other dihydroxybenzene derivatives due to overoxidation of phenol. Based on these results, a molar ratio of 1:3 (benzene to H_2O_2) afforded efficient CuFe-400 catalytic performance. The influence of the reaction time on the conversion and product selectivity over the CuFe-400 catalyst sample is shown in Fig. 5c. The conversion of benzene gradually increased from the initiation of the reaction to 6 h, and then plateaued at 6–8 h with a maximum conversion of 62%. At 62% benzene conversion, the phenol selectivity was 61%, and the other over-oxidation products that accumulated constituted 39%. The nano-CuFe-400 catalyst also exhibited excellent recyclability performance for 3 reaction cycles (Fig. 5d). The benzene conversion stabilized at 43–45% after each reaction cycles consisting of 4 h in length. In addition, the selectivity towards phenol did not change during the catalyst re-use period. More importantly, the easy recyclability of the nano-oxide CuFe composite using the external magnet makes the catalyst attractive for mediating catalyzed benzene hydroxylation for the synthesis of phenol.

4. Conclusions

In conclusion, we demonstrated that the mixed oxides of Cu and Fe result in a highly active catalyst for benzene hydroxylation for the synthesis of phenol. In addition, the activity of the CuFe catalyst depended on the calcination temperature, which significantly influenced the evolution of its structural characteristics. The correlation of the catalyst performance with the characterization results demonstrated that the formation of a $CuFe_2O_4$ spinel structure phase was not the primary requirement for obtaining a highly active and selective catalyst. However, the CuFe calcined at 400 °C with this spinel phase exhibited the best performance. Under optimized reaction conditions, the CuFe-400 catalyst afforded a benzene conversion of 44% at a combined phenol selectivity of 91%. The enhanced activity of CuFe-400 along with a H_2O_2 oxidant provides a green synthetic route for benzene hydroxylation.

Acknowledgments

The authors are grateful for financial support from the CSIR, DST and NRF. The NCNSM characterization unit is acknowledged for assisting with FESEM and TEM analyses.

Appendix A. Supplementary data

Supplementary data associated with this article can be found, in the online version, at http://dx.doi.org/10.1016/j.molcata.2014.11.023.

References

[1] R. Bal, S.A. Shankha, B. Sarkar, K. Singh Rawat, C. Pendem, Process for the selective hydroxylation of benzene with molecular oxygen, US Patent, 2013/0096351 A1.
[2] C.A. Antonyraj, K. Srinivasan, Catal. Surv. Asia 17 (2013) 47–70.
[3] M. Bahidsky, M. Hronec, Pet. Coal 46 (2004) 49–55.
[4] R.J. Schmidt, Appl. Catal. A: Gen. 280 (2005) 89–103.
[5] V. M. Zakoshansky, K. Griaznov, I.L. Vasilieva, J.W. Fulmer, W.D. Kight, Cumene oxidation process, US Patent 5.767,322 (1988).
[6] T. Jiang, W. Wang, B. Han, New J. Chem. 37 (2013) 1654–1664.
[7] R. Navarro, S. Lopez-Pedrajas, D. Luna, J.M. Marinas, F.M. Bautista, Appl. Catal. A: Gen. 22 (2014) 272–279.
[8] S. Huixian, Z. Tianyong, L. Bin, W. Xiao, H. Meng, Q. Mingyan, Catal. Commun. 12 (2011) 1022–1026.
[9] G. Ding, W. Wang, T. Jiang, B. Han, H. Fan, G. Yang, ChemCatChem. 5 (2013) 192–200.
[10] W. Jiang, W. Zhu, H. Li, Y. Chao, S. Xun, Y. Chang, H. Liu, Z. Zhao, J. Mol. Catal. A: Chem. 382 (2014) 8–14.
[11] Y. Wang, H. Zhao, M. Li, J. Fan, G. Zhao, Appl. Catal. B: Environ. 147 (2014) 534–545.
[12] D. Bianchi, M. Bertoli, R. Tassinari, M. Ricci, R. Vignola, J. Mol. Catal. A: Chem. 200 (2000) 111–116.
[13] S. Song, H. Yang, R. Rao, H. Liu, A. Zhang, Appl. Catal. A: Gen. 375 (2010) 265–271.
[14] H.H. Monfared, Z. Amouei, J. Mol. Catal. A: Chem. 217 (2004) 161–164.
[15] Y. Jiang, K. Lin, Y. Zhang, J. Liu, G. Li, J. Sun, X. Xu, Appl. Catal. A: Gen. 445–446 (2012) 172–179.
[16] G. Tanarungsun, W. Kiatkittipong, P. Praserthdam, H. Yamada, T. Tagawa, S. Assabumrungrat, Catal. Commun. 9 (2008) 1886–1890.
[17] K. Sun, H. Xia, Z. Feng, R. van Santen, E. Hensen, C. Li, J. Catal. 254 (2008) 383–396.
[18] N.K. Renuka, J. Mol. Catal. A: Chem. 316 (2010) 126–130.
[19] P.R. Makgwane, S.S. Ray, Catal. Commun. 54 (2014) 118–123.
[20] L.L. Chng, N. Erathodiyil, J.Y. Ying, Acc. Chem. Res. 46 (2013) 1825–1837.
[21] R.S. Devan, R.A. Patil, J.-H. Lin, Y.-R. Ma, Adv. Funct. Mater. 22 (2012) 3326–3370.
[22] Q. Fu, F. Yang, X. Bao, Acc. Chem. Res. 46 (2013) 1692–1701.
[23] C.-H. Cui, S.-H. Yu, Acc. Chem. Res. 46 (2013) 1427–1437.
[24] A.R. Silva, J. Botelho, J. Mol. Catal. A: Chem. 381 (2014) 171–178.
[25] G.S. Machado, F. Wypych, S. Nakagaki, Appl. Catal. A: Gen. 413–414 (2012) 94–102.
[26] G. Huang, Z.-C. Luo, Y.-D. Hu, Y.-A. Guo, Y.-X. Jiang, S.-J. Wei, Chem. Eng. J. 195-196 (2012) 165–172.
[27] R. Li, H. Kobayashi, X. Yan, J. Fan, Catal. Today 233 (2014) 140–146.
[28] A. Rostami, B. Tahmasbi, F. Abedi, Z. Shokri, J. Mol. Catal. A: Chem. 378 (2013) 200–205.
[29] C.M. Chanquía, A.L. Cánepa, J. Bazán-Aguirre, K. Sapag, E. Rodríguez-Castellón, P. Reyes, E.R. Herrero, S.G. Casuscelli, G.A. Eimer, Microporous Mesoporous Mater. 151 (2012) 2–12.
[30] A.L. Cánepa, C.M. Chanquía, G.A. Eimer, S.G. Casuscelli, Appl. Catal. A: Gen. 462–463 (2013) 8–14.
[31] G. Lin, W. Jia, W. Lu, L. Jiang, J. Colloid Interface Sci. 353 (2011) 392–397.
[32] Z. Ye, L. Hu, J. Jiang, J. Tang, X. Cao, H. Gu, Catal. Sci. Technol. 2 (2012) 1146–1149.
[33] M. Zhu, G. Diao, Catal. Sci. Technol. 2 (2012) 82–84.
[34] C.-J. Jia, F. Schüth, Phys. Chem. Chem. Phys. 13 (2011) 2457–2487.
[35] S.-C. Yang, W.-N. Su, S.D. Lin, J.-H. Cheng, J.-Y. Liu, C.-J. Pan, D.-G. Liu, J.-F. Lee, T.-S. Chan, H.-S. Sheu, B.-J. Hwang, Appl. Catal. B: Environ. 106 (2011) 650–656.
[36] F. Kenfack, H. Langbein, Cryst. Res. Technol. 39 (2004) 1070–1079.
[37] K. Yan, A. Chen, Fuel 115 (2014) 101–108.
[38] K. Xiao, Z. Bao, X. Qi, X. Wang, L. Zhong, K. Fang, M. Lin, Y. Sun, J. Mol. Catal. A: Chem. 378 (2013) 319–325.
[39] F. Wang, J. Xu, X. Li, J. Gao, L. Zhou, R. Ohnishi, Adv. Synth. Catal. 347 (2005) 1987–1992.
[40] R. Parella, N.A. Kumar, S.A. Babu, Tetrahedron Lett. 54 (2013) 1738–1742.
[41] S. Yang, C. Wu, H. Zhou, Y. Yang, Y. Zhao, C. Wang, W. Yang, J. Xua, Adv. Synth. Catal. 355 (2013) 53–58.
[42] X. Liang, X. Wang, J. Zhuang, Y. Chen, D. Wang, Y. Li, Adv. Funct. Mater. 16 (2006) 1805–1813.
[43] Z. Xiao, S. Jin, X. Wang, W. Li, J. Wang, C. Liang, J. Mater. Chem. A 22 (2012) 16598–16605.